Hindawi Publishing Corporation
International Journal of Photoenergy
Volume 2012, Article ID 838231, 11 pages
doi:10.1155/2012/838231

Research Article

PV Power-Generation System with a Phase-Shift PWM Technique for High Step-Up Voltage Applications

Cheng-Tao Tsai and Sin-Hua Chen

Department of Electrical Engineering, National Chin-Yi University of Technology, Taichung 411, Taiwan

Correspondence should be addressed to Cheng-Tao Tsai, cttsai@ncut.edu.tw

Received 14 February 2012; Accepted 20 June 2012

Academic Editor: F. Yakuphanoglu

A PV power-generation system with a phase-shift pulse-width modulation (PWM) technique for high step-up voltage applications is proposed. The proposed power-generation system consists of two stages. In the input stage, all power switches of the full-bridge converter with phase-shift technique can be operated with zero-current switching (ZCS) at turn-on or turn-off transition. Hence, the switching losses of the power switches can be reduced. Then, in the DC output stage, a voltage-doubler circuit is used to boost a high dc-link bus voltage. To supply a utility power, a dc/ac inverter is connected to induce a sinusoidal source. In order to draw a maximum power from PV arrays source, a microcontroller is incorporated with the perturbation and observation method to implement maximum power point tracking (MPPT) algorithm and power regulating scheme. In this study, a full load power of 300 W prototype has been built. Experimental results are presented to verify the performance and feasibility of the proposed PV power-generation system.

1. Introduction

To overcome fossil energy shortage and reduce air pollution, the demand of renewable energy sources has been increased significantly. One of these sources is PV arrays energy, which is clean, quiet, and maintenance-free [1, 2]. In practice, the output voltage level of PV arrays is usually much lower than that of high dc-link bus voltage. This means that a front-end dc/dc converter is required to boost the low voltage of the PV arrays to a standard high dc-link bus voltage before being inverted into a 110 V_{ac} (or 220 V_{ac}) output. Thus, the dc/dc converter with a high step-up voltage ratio and high efficiency is usually demanded. Furthermore, to obtain maximum power from PV modules, tracking the maximum power point (MPP) of PV arrays is also an essential part of the PV power system, which is mostly realized by a microcontroller with a perturbation and observation method [3–5].

To achieve a high step-up voltage ratio, high efficiency, and galvanic isolation, a voltage-fed phase-shift full-bridge converter is used as a common solution [6–11]. However, it has several disadvantages, such as large input current ripple, large circulation current and high conduction losses of power switches. Compared with the voltage-fed phase-shift full-bridge converter, the current-fed phase-shift full-bridge converter has the clear advantages of lower input-current-ripple and less conduction losses of power switches in the low-input high-output voltage conversion system. In this paper, a PV power-generation system with a current-fed phase-shift full-bridge converter for high step-up voltage applications is proposed, as shown in Figure 1. The proposed PV power-generation system has features as follows. (1) MPPT feature can be realized by a microcontroller with perturbation and observation method. (2) DC power from the PV arrays can induce a utility power via a dc/ac inverter. (3) Zero-current switching (ZCS) technology is implemented for all power switches (4) Electricity isolation is naturally obtained.

The operational principle of the proposed PV power-generation system is described in Section 2. The MPPT control scheme and protection circuit of the proposed PV power-generation system are described in Section 3. The design considerations of key components are described in Section 4. Experimental results obtained from a 300 W

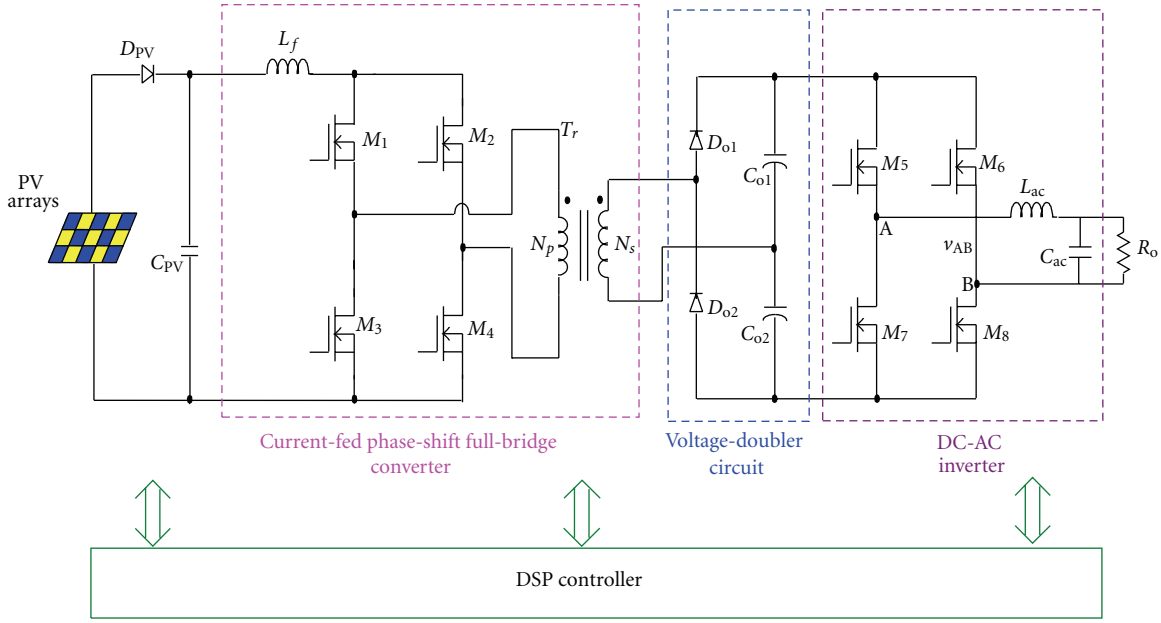

Figure 1: Circuit structure of the proposed PV power system for high step-up applications.

prototype with the proposed power-generation system for PV arrays source are presented in Section 5. Finally, a conclusion is given in Section 6.

2. Operational Principle

The circuit structure of the proposed PV power system is shown in Figure 1, in which it is composed of a current-fed phase-shift full-bridge converter, a voltage-doubler circuit and a dc-ac inverter in cascade connection. By adopting a digital signal processor (DSP) control scheme with the perturbation and observation method [12–16], the proposed PV power system can draw power from the PV arrays source with MPPT features, and feed the drawn power to the voltage-doubler circuit. Then, the dc-ac inverter operated with sinusoidal pulse-width modulation (SPWM) control scheme will generate a utility power [17–20]. For convenience of illustration and analysis, the proposed PV power-generation system shown in Figure 1 is redrawn in Figure 2.

To facilitate the analysis of operation, Figure 3 shows the driving signal of switches ($M_1 \sim M_4$) and conceptual current and voltage waveforms of key components. Figure 4 shows the topological stages of the proposed power supply system during a switching cycle. To simplify the description of the operational modes, the following assumptions are made.

(1) Boost inductor L_f is large enough so that the current flowing through it is constant over a switching period.

(2) All of the switching devices and components are ideal.

Based on the above assumptions, the operational principle can be explained mode by mode as follows.

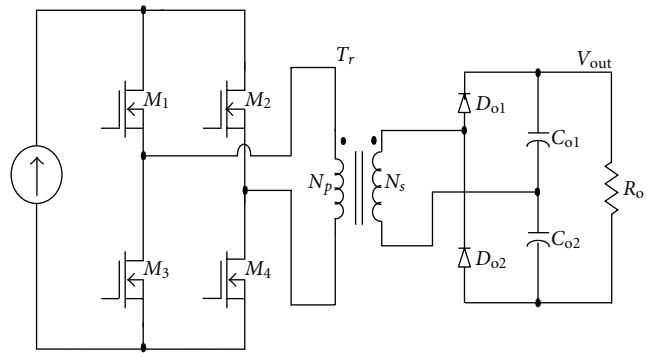

Figure 2: Simplified circuit diagram of the proposed PV power-generation system.

Mode 1 (Figure 4(a), $t_0 \le t < t_1$). This mode begins when power switches M_1 and M_4 are turned on at time t_0, and input current i_f starts to flow from the PV arrays through the transformer primary winding. At this operation, there will be a voltage across the secondary winding, which will turn on D_{o1}. Then, the current in the secondary winding will flow through C_{o1} and the load. The equivalent circuit of Mode 1 is shown in Figure 4(a).

Mode 2 (Figure 4(b), $t_1 \le t < t_2$). At time instant t_1, M_2 is turned on and M_1 as well as M_4 are still kept on but no current flows through M_1. The input current i_f is free-wheeling through power switches M_2 and M_4 and no current will flow through the transformer windings. Diodes D_{o1} and D_{o2} in secondary side of the transformer will be turned off, since all of transformer winding voltages are clamped to zero. The equivalent circuit of Mode 2 is shown in Figure 4(b).

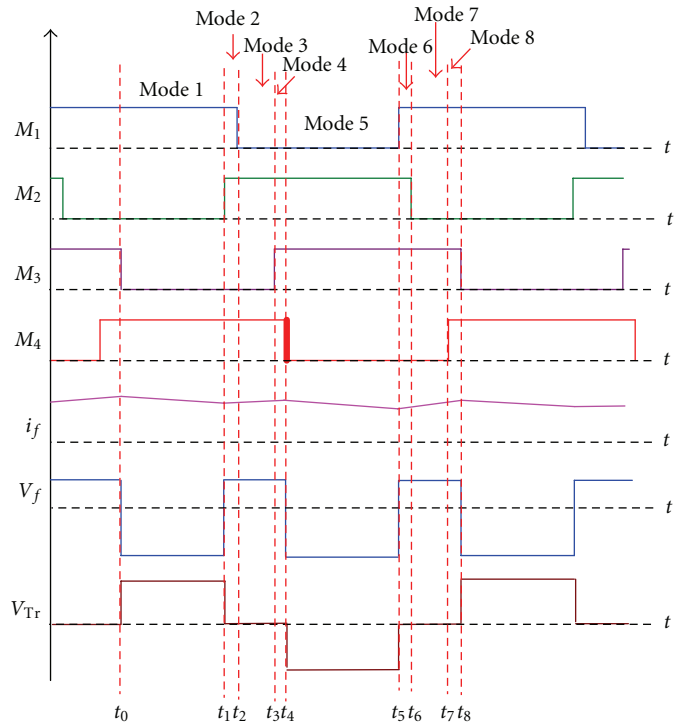

FIGURE 3: Driving signal of switches (M_1~M_4) and conceptual current and voltage waveforms of key components.

Mode 3 (Figure 4(c), $t_2 \le t < t_3$). At time instant t_2, power switch M_1 is turned off at zero current due to the reason that there is no conducted current in the previous operating stage. That is, M_1 is operated with ZCS at turn-off transition. The power switches M_2 and M_4 are maintained on, and input current i_f is continuous free-wheeling through M_2 and M_4. The equivalent circuit of Mode 3 is shown in Figure 4(c).

Mode 4 (Figure 4(d), $t_3 \le t < t_4$). At time instant t_3, power switches M_2 and M_4 are still kept on. Power switch M_3 is turned on and operated with ZCS at turn-on transition, because transformer winding has no voltage. The equivalent circuit of Mode 4 is shown in Figure 4(d).

Mode 5 (Figure 4(e), $t_4 \le t < t_5$). At time instant t_4, power switches M_2 and M_3 are still kept on and M_4 is turned off. The input current i_s starts to revise flowing through the transformer primary winding. At this operation, there will be a revised voltage across the secondary winding of transformer which will turn on D_{o2}. Thus, the current in the secondary winding will flow through C_{o2} and the load. The equivalent circuit of Mode 5 is shown in Figure 4(e).

Mode 6 (Figure 4(f), $t_5 \le t < t_6$). At time instant t_5, M_2 and M_3 are still kept on and M_1 is turned on. The input current i_f is free-wheeling through power switches M_1 and M_3 and no current will flow through the transformer windings. Diodes D_{o1} and D_{o2} in the transformer secondary will be turned off once again, since all of transformer winding voltages are clamped to zero. The equivalent circuit of Mode 6 is shown in Figure 4(f).

Mode 7 (Figure 4(g), $t_6 \le t < t_7$). At time instant t_6, M_1 and M_3 are still kept on and M_2 is turned off. Power switch M_2 is turned off under ZCS condition, due to the reason that there is no conducted current in the previous operating stage. The equivalent circuit of Mode 7 is shown in Figure 4(g).

Mode 8 (Figure 4(h), $t_7 \le t < t_8$). At time instant t_7, M_1 and M_3 are still kept on and M_4 is turned on and operated with ZCS at turn-on transition, because transformer winding has no voltage. The equivalent circuit of Mode 8 is shown in Figure 4(h). The proposed power system operation over one switching cycle is completed.

3. Control Scheme of MPPT

The PV arrays are constructed by many series or parallel connected solar cells. Each solar cell is formed by a P-N junction semiconductor, which can produce currents by the photovoltaic effect. The typical *V-I* and output power characteristic curves of the PV arrays with different insolations are shown in Figure 5. For a specific isolation, there exists one operating point where the PV array can generate its maximum output power. In order to achieve the best energy utilization of the PV arrays, an MPPT algorithm must be integrated into the control strategy of the current-mode phase-shift full-bridge converter.

Figure 6 illustrates the flow chart of the MPPT algorithm. First of all, the terminal voltage V_{PV} and current I_{PV} of PV arrays are measured. The output power of PV arrays P_{PV} can be obtained from the product of V_{PV} and I_{PV}.

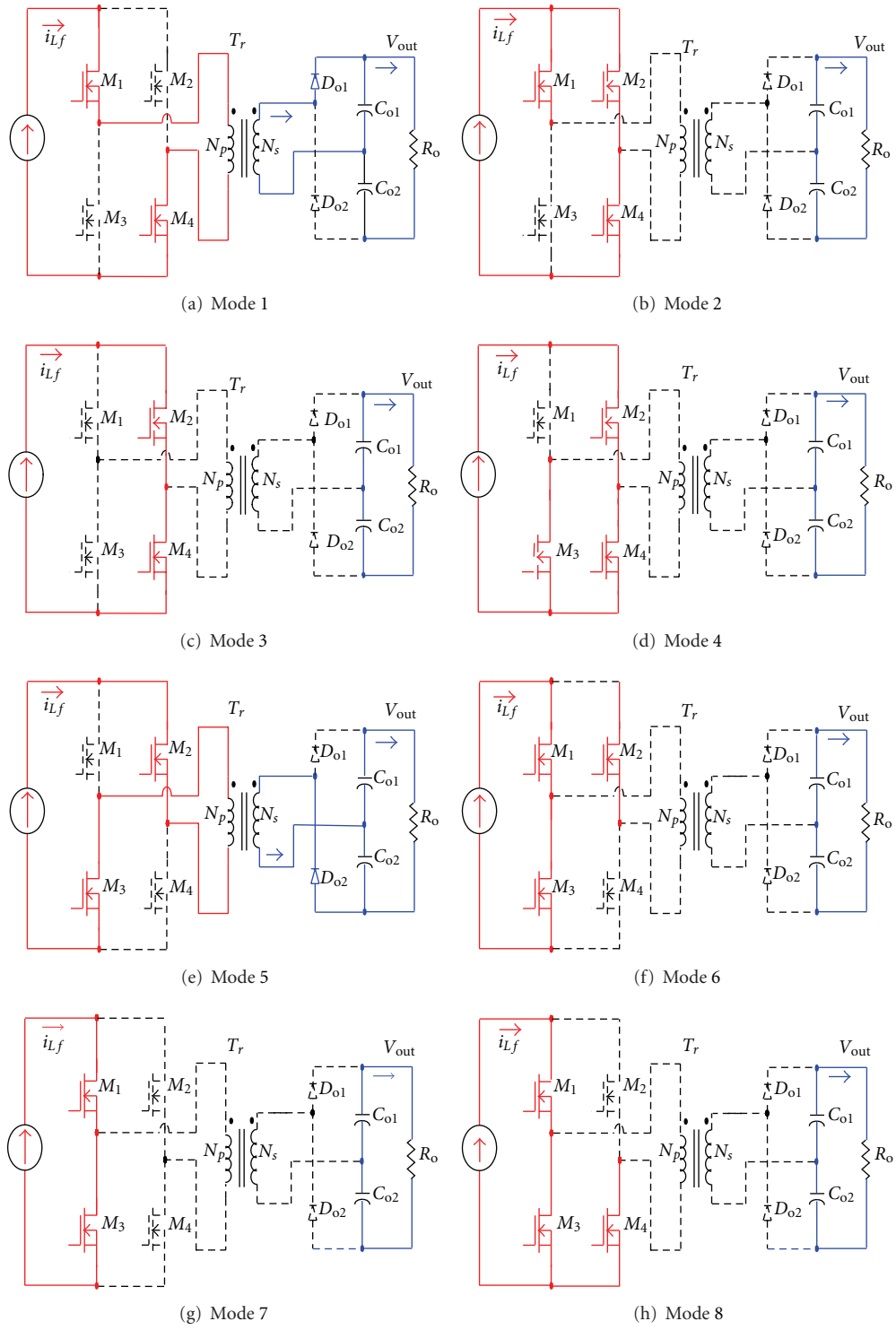

Figure 4: Equivalent circuits of operating modes.

From the plot of P_{PV} versus V_{PV}, as shown in Figure 7, two possible operating regions A and B for a given P_{PV} except the maximum power point can be defined. The current operating point location can be determined by a perturbation in the PV output power. For instance, the output power and terminal voltage of PV arrays with a perturbation are found to be

$$P_{PV}(n-1) = P_2 < P_{PV}(n) = P_1,$$
$$V_{PV}(n-1) = V_2 > V_{PV}(n) = V_1, \quad (1)$$

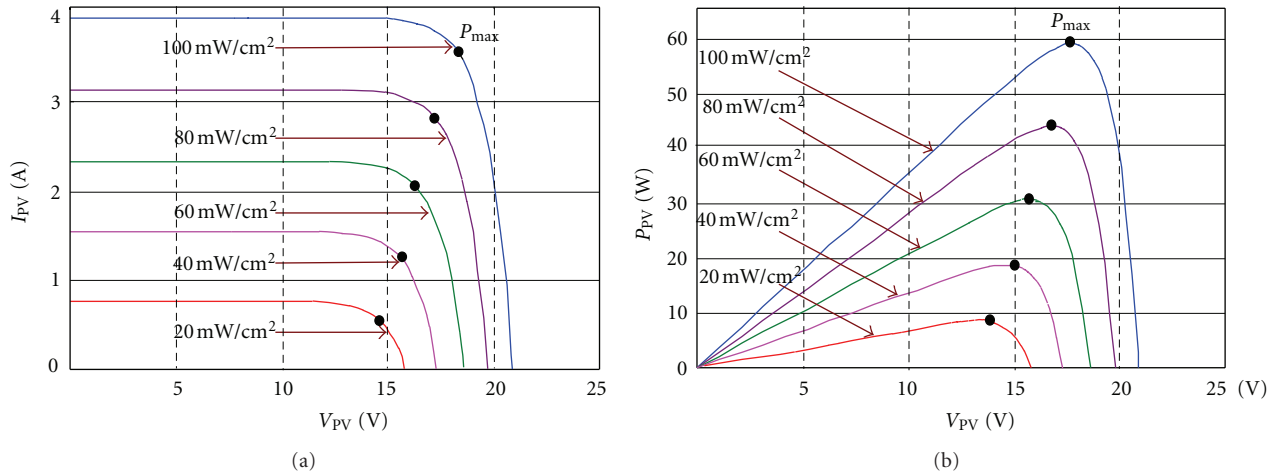

Figure 5: PV arrays with different insolations: (a) *V-I* curves, and (b) output power and output voltage curves.

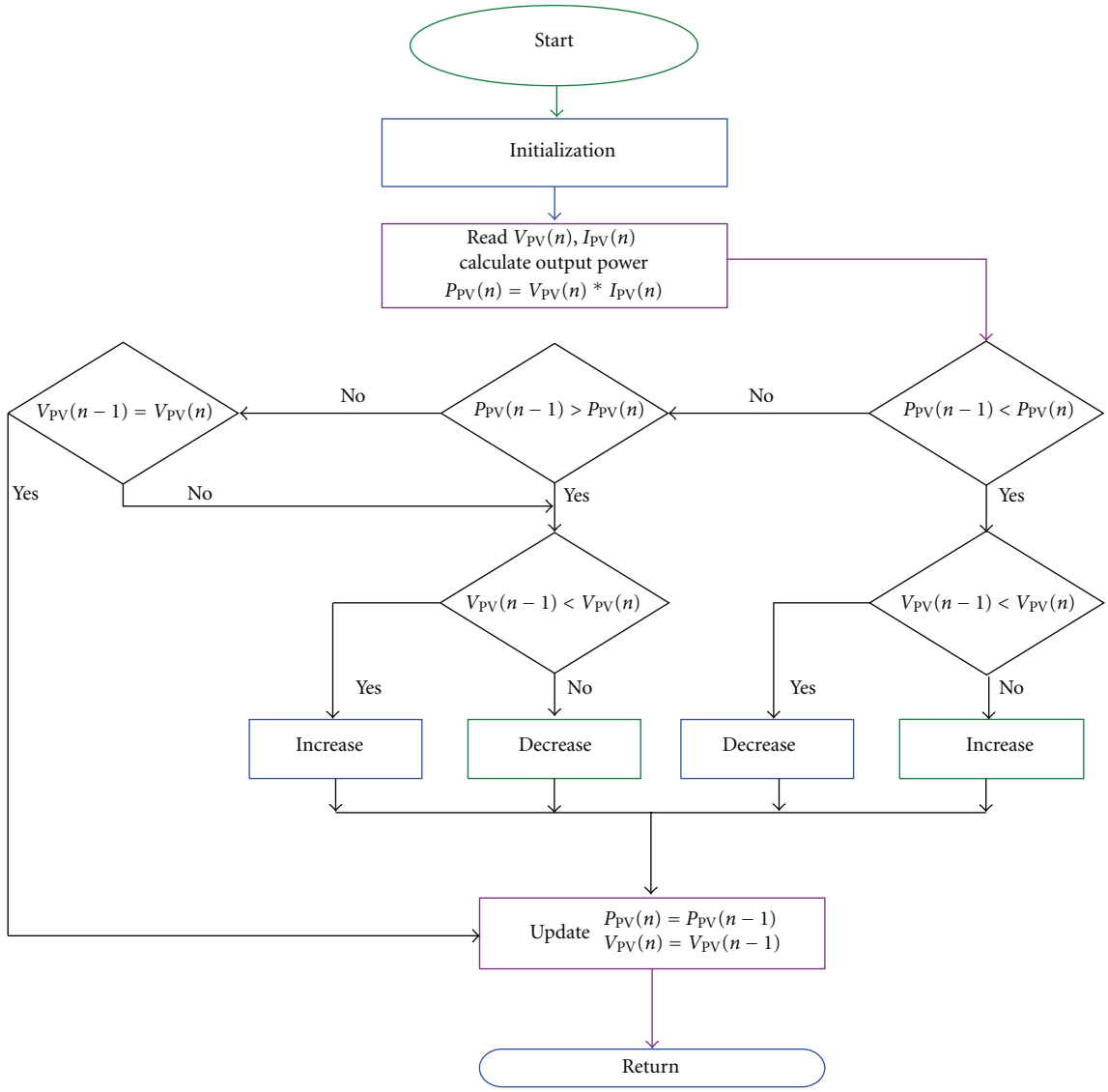

Figure 6: Flow chart of perturbation and observation method for MPPT algorithm.

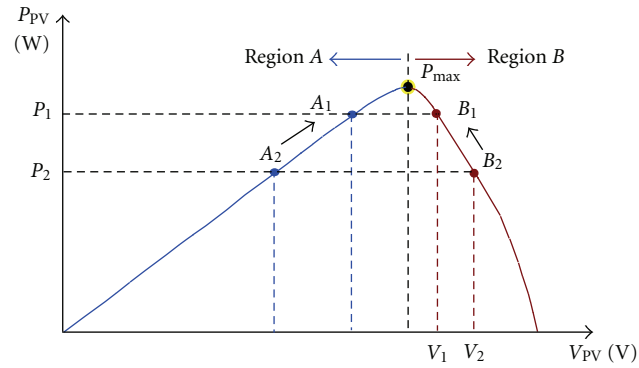

Figure 7: PV output power curve with respect to the PV output voltage.

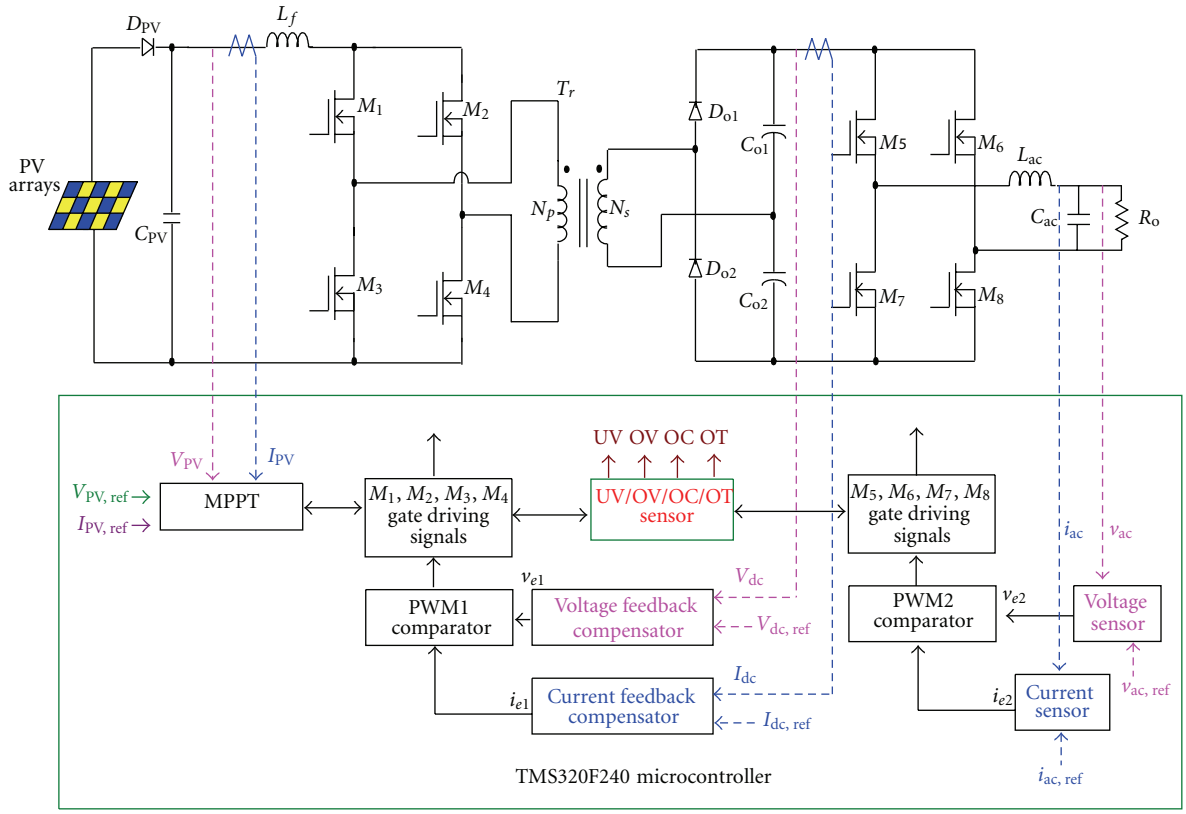

Figure 8: Conceptual control block diagram of the proposed PV power-generation system.

where parameters $n-1$ and n indicate the measured quantities before and after the perturbation, respectively. Equation (1) imply that this perturbation leads to an increased P_{PV} and a decreased V_{PV}. From the program flow chart shown in Figure 6, it can be determined that the correct operating point of PV arrays is currently located in region B. Thus, to track the maximum power point for PV arrays, the next changing direction is to increase load, resulting in a reduction of V_{PV}. Hence, the operating point is moving from B_2 to B_1 in Figure 7. If the correct operating point of PV arrays is currently located in region A, then the next changing direction is to decrease load. Hence, the operating point will be moved from A_2 toward A_1. With this continuous process, the operating point of PV arrays can be moved toward the maximum power point for different temperature and insolation conditions. In this study, the MPPT algorithm mentioned above is realized on a single-chip microprocessor TMS320F240.

In order to regulate the output voltage of the proposed PV power-generation system and provide high-quality ac power to the load, the effective voltage and current feedback compensators are essential. By processing of feedback compensators, the voltage error signal v_{e1} and current error signal i_{e1} will be obtained. Then, the PWM1 compensator will

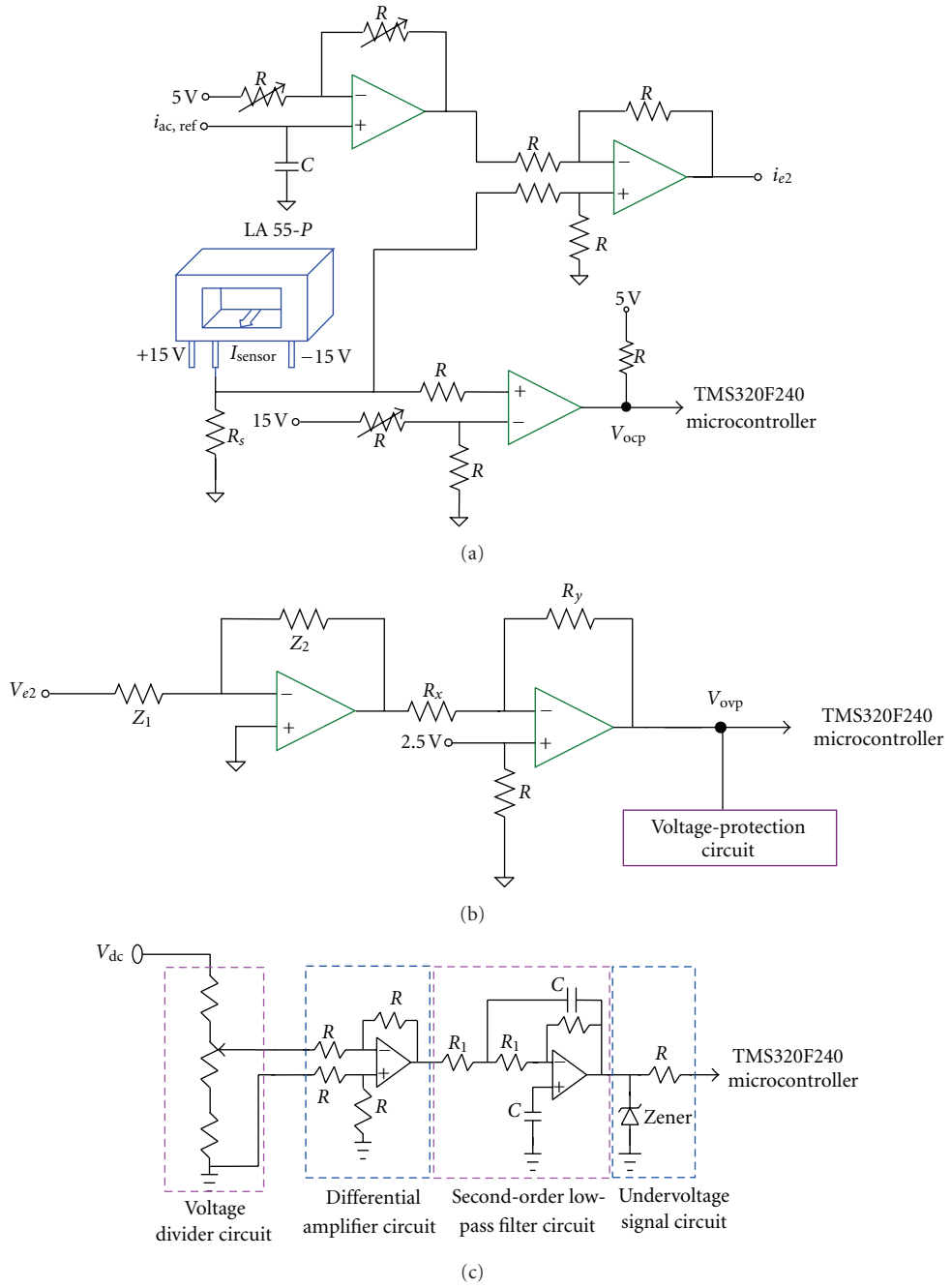

Figure 9: Protection circuits of the inverter: (a) overcurrent protection circuit, (b) overvoltage protection circuit, and (c) under voltage protection circuit.

generate driving signals of switches ($M_1 \sim M_4$) to regulate the dc output voltage. The output voltage of inverter v_{ac} and its filter inductor current i_{ac} are sampled to generate driving signals of switches ($M_5 \sim M_8$) and employed to realize a high steady and dynamic response sinusoidal voltage. The control strategies can be implemented by the TMS320F240 microcontroller to improve the system performance. The conceptual control block diagram of the proposed PV power-generation system is shown in Figure 8.

To achieve an optimal stability and safety for the proposed PV power-generation system, the functions of undervoltage, overvoltage protection, overcurrent protection, and overtemperature protection are required. Figures 9 and 10 show the key protection circuits of the proposed PV power-generation system. All of the protection signals are also realized on the TMS320F240 microcontroller, as shown in Figure 8.

4. Design Considerations of Power Switches

Most power converters have power components that operate at temperatures that are high enough to cause burns

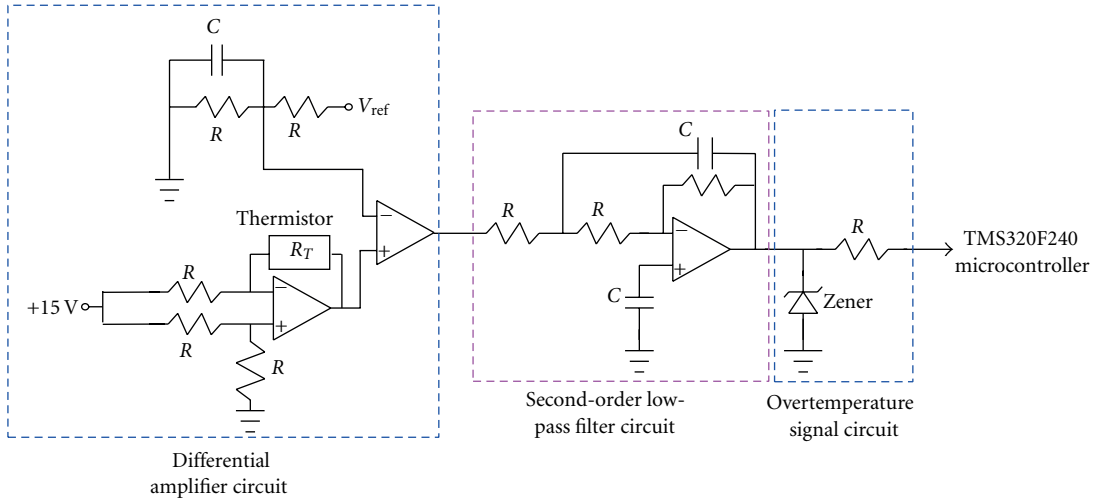

Figure 10: Over-temperature protection circuit of the proposed PV power-generation system.

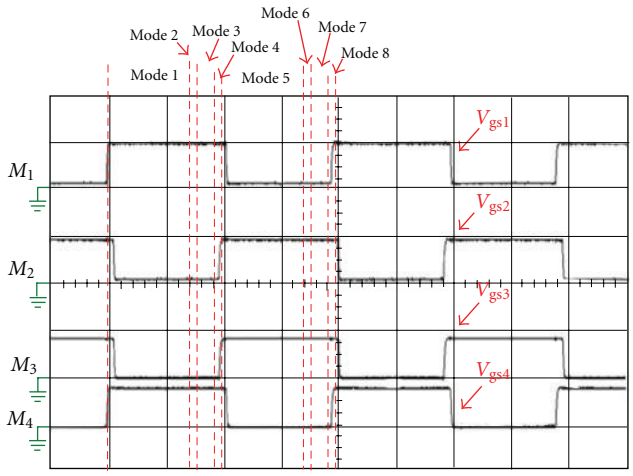

($V_{gs1} \sim V_{gs4}$: 20 V/div; time: 5 μs/div)

Figure 11: Measured gate signal waveforms of the power switches ($M_1 \sim M_4$).

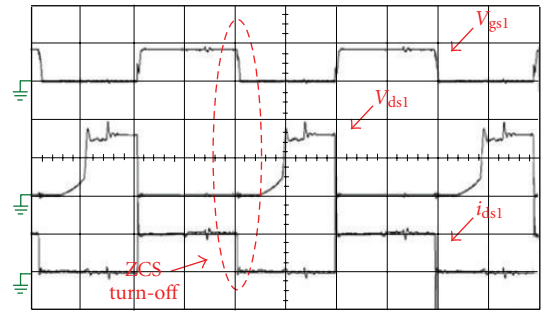

(V_{gs1}: 20 V/div; V_{ds1}: 20 V/div; i_{ds1}: 10 A/div; time: 5 μs/div)

Figure 12: Measured voltage and current waveforms of the power switch M_1.

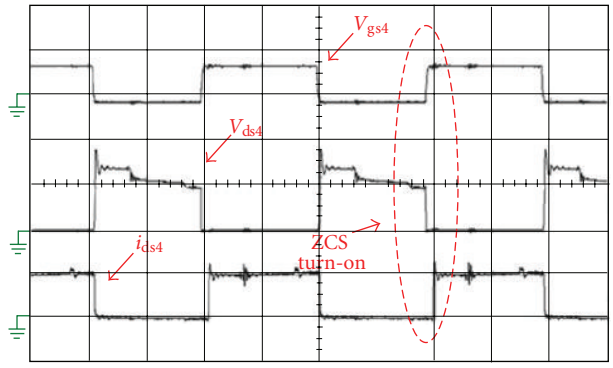

(V_{gs4}: 20 V/div; V_{ds4}: 20 V/div; i_{ds4}: 10 A/div; time: 5 μs/div)

Figure 13: Measured voltage and current waveforms of the power switch M_4.

if handled improperly. The power dissipation in power switches normally increases with the internal temperature, and the losses become excessively high even at temperatures of 200°C. Component manufacturers typically will guarantee the maximum values of component parameters such as onstate conduction voltages, switching frequencies, and switching losses at a specified maximum temperature, which varies from one type of component to another and is often at 125°C. Therefore, a system intended to have high reliability would be designed for a worse-case junction temperature in power switches of 20–40°C below 125°C. In order to reduce temperatures of the power switches for the proposed PV power-generation system, the small heat sinks are usually recommended.

The proposed PV power-generation system consists of a phase-shift full-bridge converter, a voltage-doubler circuit, and a full-bridge inverter, as shown in Figure 1. To design the proposed PV power-generation system, their power switches are considered in the following.

4.1. Selection of the Power Switches ($M_1 \sim M_4$). For the current-fed full-bridge phase-shift converter, the voltage

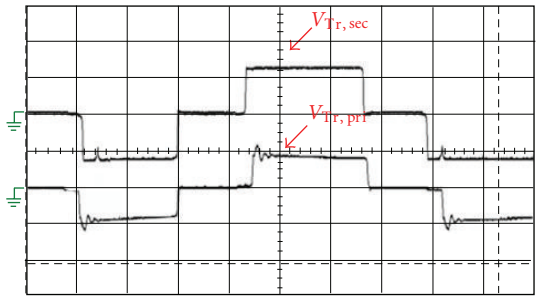

($V_{Tr,pri}$: 20 V/div; $V_{Tr,sec}$: 100 V/div; time: 2 μs/div)

FIGURE 14: Measured primary and secondary voltage waveforms of the transformer.

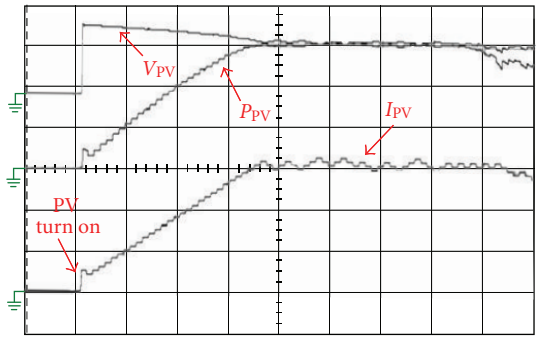

(V_{PV}: 20 V/div; I_{PV}: 5 A/div; P_{PV}: 10 W/div; time: 5 s/div)

FIGURE 15: Measured output voltage, current, and power waveforms of PV arrays.

stress imposed on power switches ($M_1 \sim M_4$) is $V_{ds(max)} = V_{PV} + V_{Lf} = 40$ V. When power switches are turned on, the maximum switching current $i_{ds(peak)}$ is equal to the current $i_{Lf(peak)}$. Thus, the maximum switching current $i_{ds(peak)} = 10$ A. Selection of power switches involves a tradeoff between conduction losses and switching losses. MOSFETs with low $R_{ds(on)}$ can usually keep low conduction losses and temperatures, but they usually have high parasitic capacitance and require a larger die size. In this design, the power switches are IRF530N with a drain-source breakdown voltage of 100 V, drain current of 15 A, and a channel resistance of 0.064 Ω.

4.2. Selection of the Power Switches ($M_5 \sim M_6$). For the dc/ac inverter, the voltage stress imposed on power switches ($M_5 \sim M_8$) is $V_{ds(max)} = V_{out} = 230$ V. When power switches are turned on, the maximum switching current $i_{ds(max)}$ is equal to 3 A. Therefore, the power switches are IRFIP350 with a drain-source breakdown voltage of 400 V, drain current of 12 A, and a channel resistance of 0.3 Ω.

4.3. Selection of the Rectifier Diodes (D_{o1}, D_{o2}). In the voltage-doubler circuit, the voltage stress imposed on rectifier diodes D_{o1} and D_{o2} is $V_{Do} = (N_s/N_p)(V_{in}/2) = 115$ V. When rectifier diode D_{o1} or D_{o2} is conducting, the maximum diode current $i_{Do(max)} = (N_p/N_s)I_{in(max)} = 0.9$ A. Thus, an MUR420 ultrafast diode which has a maximum recurrent peak reverse voltage of 200 V, maximum average forward rectified current of 4 A, and forward voltage drop ($V_F = 0.89$ V) is selected.

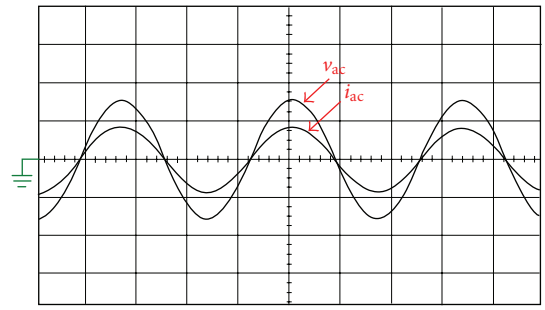

(V_{ac}: 100 V/div; i_{ac}: 5 A/div, time: 5 ms/div)

FIGURE 16: Measured ac output voltage and current waveforms of inverter.

5. Experimental Results

To verify the performance of the proposed PV power-generation system, a 300 W prototype power system was built. Its specifications are listed as follows:

(1) input voltages: $V_{PV} = 15 \sim 20\ V_{dc}$,

(2) dC output voltage: $V_{dc} = 230\ V_{dc}$,

(3) output AC voltage: $v_{ac} = 110\ V_{ac}$, 60 Hz,

(4) output power: $P_{o,max} = 300$ W,

(5) switching frequency: $f_s = 50$ kHz ($M_1 \sim M_4$),

(6) switching frequency: $f_{sac} = 20$ kHz ($M_5 \sim M_6$).

Figure 11 shows measured gate signal waveforms of power switches ($M_1 \sim M_4$). Figures 12 and 13 show measured drain-source voltage and current waveforms of the power switches M_1 and M_4 to illustrate a ZCS feature at turn-on or turn-off transition, respectively. In Figures 12 and 13, ringing condition appeared in voltage and current waveforms of power switches are caused by the parasitic elements of the switching devices and the transformer. Figure 14 shows measured primary and secondary voltage waveforms of transformer. Figure 15 shows measured output current, voltage, and their corresponding power from start-up to the steady state for PV with MPPT algorithm. It can be observed that the MPPT feature for the PV can be always achieved even though the output power of the PV is altered. Figure 16 shows measured inverter voltage and current waveforms under full load 300 W condition, from which it can be seen obviously that the inverter output voltage and current are sinusoidal. By using the power analyzer Voltech PM100, a power factor of 0.99 and a THD of inverter output current less than 3% are measured. For practical applications, many circuit protection functions are included in the hardware realization. Some of the testing waveforms are shown in Figure 17. Figure 17 shows measured waveforms of over-voltage, under-voltage, and over-current protection for the proposed power-generation system. From Figure 17, it can be seen that the power-generation system will be shut-down

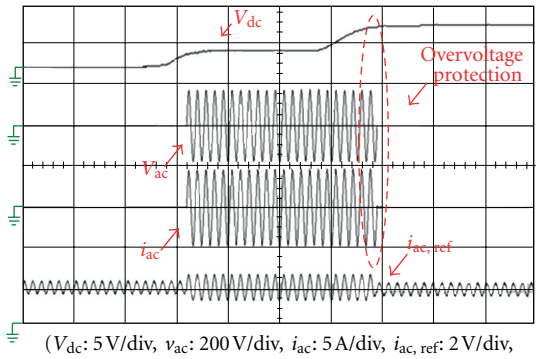

(V_{dc}: 5 V/div, v_{ac}: 200 V/div, i_{ac}: 5 A/div, $i_{ac,ref}$: 2 V/div, time: 100 ms/div)

(a)

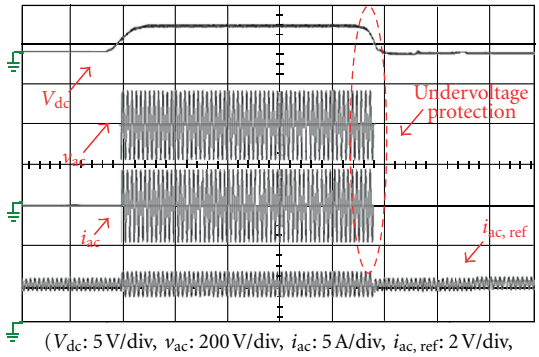

(V_{dc}: 5 V/div, v_{ac}: 200 V/div, i_{ac}: 5 A/div, $i_{ac,ref}$: 2 V/div, time: 200 ms/div)

(b)

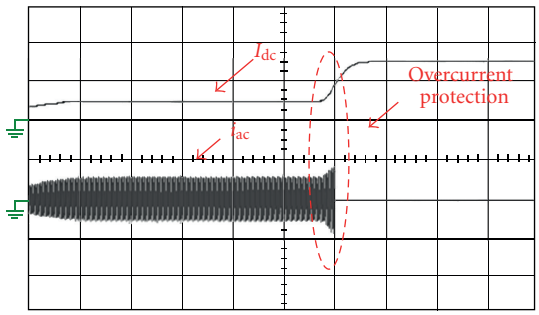

(I_{dc}: 5 V/div, i_{ac}: 5 A/div, time: 500 ms/div)

(c)

Figure 17: Measured waveforms for circuit protection functions: (a) over-voltage protection, (b) under-voltage protection, and (c) over-current protection.

protection at once when the value of the V_{dc} or I_{dc} is beyond the preset range.

6. Conclusions

In this paper, a PV power-generation system for high step-up voltage applications is proposed. All power switches of the full-bridge converter with phase-shift PWM technique have a ZCS feature at turn-on or turn-off transition. Hence, the switching losses of the power switches can be reduced. In order to draw maximum power from the PV arrays source, a simple perturbation and observation method is incorporated to realize maximum power conversion. Then, the dc-link bus is used by a dc/ac inverter, which can induce a sinusoidal source to supply utility power. To adopt a cost effective of the proposed power supply system, the MPPT algorithms and protected circuits consist of a digital signal processor (DSP) and analog circuits to implement MPPT and protect system. Thus, the control circuit of the proposed PV power-generation system is compact and programmable. Experimental results have been verified that the proposed PV power-generation system is relatively suitable for high step-up voltage applications.

References

[1] S. R. Bull, "Renewable energy today and tomorrow," *Proceedings of the IEEE*, vol. 89, no. 8, pp. 1216–1226, 2001.

[2] S. Jemeï, D. Hissel, M. C. Péra, and J. M. Kauffmann, "A new modeling approach of embedded fuel-cell power generators based on artificial neural network," *IEEE Transactions on Industrial Electronics*, vol. 55, no. 1, pp. 437–447, 2008.

[3] K. H. Hussein, I. Muta, T. Hoshino, and M. Osakada, "Maximum photovoltaic power tracking: an algorithm for rapidly changing atmospheric conditions," *IEE Proceedings*, vol. 142, no. 1, pp. 59–64, 1995.

[4] S. Wakao, R. Ando, H. Minami et al., "Performance analysis of the PV/Wind/ Wave hybrid power generation system," in *Proceddings of the 3rd World Conference on Photovoltaic Energy Conversion*, pp. 2337–2340, May 2003.

[5] H. J. Chiu, H. M. Huang, L. W. Lin, and M. H. Tseng, "A multiple-input DC/DC converter for renewable energy systems," in *Proceddings of the IEEE International Conference on Industrial Technology (ICIT '05)*, pp. 1304–1308, December 2005.

[6] Y. Jang and M. M. Jovanović, "A new family of full-bridge ZVS converters," *IEEE Transactions on Power Electronics*, vol. 19, no. 3, pp. 701–708, 2004.

[7] E. H. Kim and B. H. Kwon, "Zero-voltage- and zero-current-switching full-bridge converter with secondary resonance," *IEEE Transactions on Industrial Electronics*, vol. 57, no. 3, pp. 1017–1025, 2010.

[8] F. Liu, J. Yan, and X. Ruan, "Zero-voltage and zero-current-switching PWM combined three-level DC/DC converter," *IEEE Transactions on Industrial Electronics*, vol. 57, no. 5, pp. 1644–1654, 2010.

[9] Y. Jang and M. M. Jovanović, "A new three-level soft-switched converter," *IEEE Transactions on Power Electronics*, vol. 20, no. 1, pp. 75–81, 2005.

[10] Y.-C. Kuo, T.-J. Liang, and J.-F. Chen, "Novel maximum-power-point-tracking controller for photovoltaic energy conversion system," *IEEE Transactions on Industrial Electronics*, vol. 48, no. 3, pp. 594–601, 2001.

[11] M. Mohr and F. W. Fuchs, "Clamping for current-fed dc/dc converters with recovery of clamping energy in fuel cell inverter systems," in *Proceedings of the European Conference on Power Electronics and Applications (EPE '07)*, pp. 1–10, September 2007.

[12] Y. C. Kuo, T. J. Liang, and J. F. Chen, "Novel maximum-power-point-tracking controller for photovoltaic energy conversion system," *IEEE Transactions on Industrial Electronics*, vol. 48, no. 3, pp. 594–601, 2001.

[13] H. Matsuo, W. Lin, F. Kurokawa, T. Shigemizu, and N. Watanabe, "Characteristics of the multiple-input dc-dc converter,"

IEEE Transactions on Industrial Electronics, vol. 51, no. 3, pp. 625–631, 2004.

[14] J. G. Cho, J. W. Baek, C. Y. Jeong, D. W. Yoo, and K. Y. Joe, "Novel zero-voltage and zero-current-switching full bridge PWM converter using transformer auxiliary winding," *IEEE Transactions on Power Electronics*, vol. 15, no. 2, pp. 250–257, 2000.

[15] Y. M. Chen, Y. C. Liu, S. C. Hung, and C. S. Cheng, "Multi-input inverter for grid-connected hybrid PV/wind power system," *IEEE Transactions on Power Electronics*, vol. 22, no. 3, pp. 1070–1077, 2007.

[16] Y. M. Chen, Y. C. Liu, and S. H. Lin, "Double-input PWM DC/DC converter for high-/low-voltage sources," *IEEE Transactions on Industrial Electronics*, vol. 53, no. 5, pp. 1538–1545, 2006.

[17] A. Koyanagi, H. Nakamura, M. Kobayashi, Y. Suzuki, and R. Shimada, "Study on maximum power point tracking of wind turbine generator using a flywheel," in *Proceedings of the Power Conversion Conference*, vol. 1, pp. 322–327, 2002.

[18] K. Amei, Y. Takayasu, T. Ohji, and M. Sakui, "maximum power control of wind generator system using a permanent magnet synchronous generator and a boost chopper circuit," in *Proceedings of Power Conversion Conference*, vol. 3, pp. 1447–11452, 2002.

[19] S. B. Kjaer, J. K. Pedersen, and F. Blaabjerg, "A review of single-phase grid-connected inverters for photovoltaic modules," *IEEE Transactions on Industry Applications*, vol. 41, no. 5, pp. 1292–1306, 2005.

[20] H. Patel and V. Agarwal, "MPPT scheme for a PV-fed single-phase single-stage grid-connected inverter operating in CCM with only one current sensor," *IEEE Transactions on Energy Conversion*, vol. 24, no. 1, pp. 256–263, 2009.